

## Article

# Machinability Comparison of TiCN-Al<sub>2</sub>O<sub>3</sub>-TiN, TiAlN-TiN, and TiAlSiN Coated Carbide Inserts in Turning Hardened AISI 4340 Steel Using Grey-Crow Search Hybrid Optimization

Mohammed Al Awadh <sup>1</sup>, Ramanuj Kumar <sup>2,\*</sup>, Oğur İynen <sup>3</sup>, Mohammad Rafighi <sup>4,\*</sup>, Mustafa Özdemir <sup>5</sup> and Anish Pandey <sup>2</sup>

<sup>1</sup> Department of Industrial Engineering, King Khalid University, Abha 61411, Saudi Arabia; mohalawadh@kku.edu.sa

<sup>2</sup> School of Mechanical Engineering, Kalinga Institute of Industrial Technology Deemed to be University, Bhubaneswar 751024, India; anish.pandeyfme@kiit.ac.in

<sup>3</sup> Department of Mechanical Engineering, Yozgat Bozok University, Yozgat 66200, Turkey; ogur.iynen@bozok.edu.tr

<sup>4</sup> Department of Mechanical Engineering, Başkent University, Ankara 06790, Turkey

<sup>5</sup> Department of Machine and Metal Technology, Yozgat Bozok University, Yozgat 66200, Turkey; mustafa.ozdemir@bozok.edu.tr

\* Correspondence: ramanujkumar22@gmail.com (R.K.); mohammad.rafighi@gmail.com (M.R.)

**Abstract:** This experimental study presents the machinability comparison of TiCN-Al<sub>2</sub>O<sub>3</sub>-TiN, TiAlN-TiN, and TiAlSiN coated carbide inserts in hard turning AISI 4340 steel. The primary purpose of this research is to determine the most appropriate cutting inserts in turning hardened AISI 4340 (30–40 HRC) steel considering surface roughness (Ra), cutting sound (Cs), power consumption (P), radial force (Fx), tangential force (Fy), and feed force (Fz). To fulfill this objective, the turning experiments for each tool were executed based on the Taguchi L<sub>9</sub> design. The comparative assessment of cutting tools revealed that the TiAlSiN coated tool exhibited superior performance compared to other tools. Machining with the TiCN-Al<sub>2</sub>O<sub>3</sub>-TiN coated tool showed 32.05% greater roughness than with the TiAlN-TiN coated tool, and 68.80% higher surface roughness than the TiAlSiN coated tool. The main novelty of this research is considering the cutting sound and power consumption as responses to select the most suitable cutting tools. Moreover, a novel grey-crow search hybrid was executed to perceive the optimal value of the input parameters. The optimal local value of cutting speed for the TiAlSiN coated tool was found to be 220 m/min, while for the TiCN-Al<sub>2</sub>O<sub>3</sub>-TiN and TiAlN-TiN tools, it was the same as 182 m/min. Considering the optimum cutting parameters, the material removal rate for TiCN-Al<sub>2</sub>O<sub>3</sub>-TiN, TiAlN-TiN, and TiAlSiN was found to be 639.9 mm<sup>3</sup>/min, 606.4 mm<sup>3</sup>/min, and 761.2 mm<sup>3</sup>/min, respectively. Thus, the TiAlSiN coated tool has greater MRR capability in comparison to other tools. Therefore, this leads to the conclusion that the TiAlSiN tool may be the better choice in comparison to other selected tools for turning hardened steels.

**Keywords:** cutting sound; power consumption; surface roughness; cutting forces; hard turning; coating



**Citation:** Al Awadh, M.; Kumar, R.; İynen, O.; Rafighi, M.; Özdemir, M.; Pandey, A. Machinability Comparison of TiCN-Al<sub>2</sub>O<sub>3</sub>-TiN, TiAlN-TiN, and TiAlSiN Coated Carbide Inserts in Turning Hardened AISI 4340 Steel Using Grey-Crow Search Hybrid Optimization. *Metals* **2023**, *13*, 973. <https://doi.org/10.3390/met13050973>

Academic Editor: Badis Haddag

Received: 24 April 2023

Revised: 15 May 2023

Accepted: 15 May 2023

Published: 17 May 2023



**Copyright:** © 2023 by the authors. Licensee MDPI, Basel, Switzerland. This article is an open access article distributed under the terms and conditions of the Creative Commons Attribution (CC BY) license (<https://creativecommons.org/licenses/by/4.0/>).

## 1. Introduction

Currently, the machining of hard materials such as steel is considered to be an alternate method for grinding, especially in the automotive, aerospace, and die-mold industries [1–3]. The process of turning involves the removal of layers of extra material from the workpiece using a sharp-wedge tool through plastic deformation followed by the shearing of the material [4,5]. Referring to the open literature report, the turning of heat-treated steel is a difficult task, as higher cutting temperatures; higher cutting forces; severe tool wear, and higher surface roughness are found due to plastic deformation followed by the shearing of material in dry cutting [6]. However, different cooling strategies were implemented in turning the hardened steel to control the machining temperature and improve the

surface finishing. The coolants helped to minimize the friction between contact surfaces and cool the shearing zone area, and as a result, the temperature was reduced, and thus tool wear was delayed and surface quality was improved. However, although the use of coolant was advantageous for machining hard steel, it results in a significant economic and ecological burden on the manufacturers. Therefore, dry cutting conditions can be used for machining hardened steel if appropriate cutting tools and suitable cutting parameters were chosen [5,6].

Due to the growing demand for the high precision and high surface quality of the machined component, the production cost was enhanced because of the need for expensive super hard cutting tools such as CBN/PCBN, and ceramics in machining heat-treated steels under dry circumstances. The efficacy of these cutting tools is superior, even at elevated cutting speeds, owing to their excellent thermo-mechanical stability, exceptional wear resistance, and higher hardness characteristics. In recent studies, in order to minimize the production cost, the use of a low budgetary tool such as a coated carbide insert was commonly found in turning hardened steel. The cutting ability of the coated carbide tool solely relies upon the features of the coating layers, cutting tool geometry, and the cutting parameter value. Globally, many researchers have implemented different ceramic coatings on carbide substrates using PVD/CVD technology to achieve improved characteristics such as heat evacuation, lesser friction, and resistance against abrasion, diffusion, and chemical interaction. The commonly used multiple layer coatings on the carbide substrate for hardened steel machining are TiAlN-TiN [7], TiSiN-TiAlN [8], TiN-AlCrN [9], Al<sub>2</sub>O<sub>3</sub>-TiC [10], Al<sub>2</sub>O<sub>3</sub>-TiCN [11], TiN-TiCN-Al<sub>2</sub>O<sub>3</sub> [12], TiC-TiCN-Al<sub>2</sub>O<sub>3</sub> [13], TiCN-Al<sub>2</sub>O<sub>3</sub>-TiN [14], TiN-Al<sub>2</sub>O<sub>3</sub>-TiCN [15], TiN-TiCN-Al<sub>2</sub>O<sub>3</sub>-TiN [16], TiN-TiCN-Al<sub>2</sub>O<sub>3</sub>-ZrCN [17], and TiC-TiCN-Al<sub>2</sub>O<sub>3</sub>-TiN [18]. However, there is still enough space to use some new coating tools in machining hardened steel.

Due to the development of recent coatings over tool substrates, the hard turning performances of these tools should be critically analyzed and compared for achieving a better cutting tool for the machining of hard steels. Abbas et al. [19] equated the enactment of the CVD tool (TiCN-Al<sub>2</sub>O<sub>3</sub>-TiN) with the wiper geometry-PVD tool (TiCN-TiN) in machining 4340 steel. The PVD tool worked better to achieve a relatively improved surface finish than the CVD tool. Similarly, Mallick et al. [20] explored the comparative concert of PVD (AlTiN) and CVD (TiCN-Al<sub>2</sub>O<sub>3</sub>) coated carbide cutting tools in machining hardened D2 grade steel. The CVD tool imparts better results, as tool life was enhanced by 14.3% in comparison to the PVD tool. Das et al. [21] equated the concert of AlTiN and AlTiSiN coated tools in turning D6 hardened steel. The AlTiSiN tool performed well and provided 47.83% greater tool life in comparison to the AlTiN tool. Boing et al. [22] also inspected the cutting performances of the PVD (TiAlN) and CVD (TiCN-Al<sub>2</sub>O<sub>3</sub>-TiN coating of two grades) tools in turning 4340 steel. The tool life of the PVD tool was very high relative to both grades of the CVD tool. Varghese et al. [23] equated the TiAlSiN and TiSiN coating tool performance in milling MDN 250 steel. The TiAlSiN tool exhibited greater resistance against wear capability than the TiSiN tool. Sousa et al. [24] found a better machining ability of the TiAlSiN tool against a TiAlN coated tool in milling hardened state tool steel workpieces. The adhesion, abrasion, and coating delamination of the tool were traced to be the major forms of wear mechanisms.

The hardness of the hardened steel plays a crucial role in identifying the suitable coated tool for machining. The tool life of the used cutting tool was substantially enhanced by the workpiece hardness [25]. Moreover, the hardness of the workpiece significantly influenced the tool wear, cutting force, surface roughness, cutting temperature [26], and chip morphology in machining hardened steel. De Lima et al. [27] achieved the abridged cutting force when the hardness of 4340 steel decreased from 50 HRC to 42 HRC. Caydas [28] stated that the roughness of the cutting surface was enhanced with the leading hardness (35 to 45 HRC) of the job, but with further increments in hardness, the surface roughness was diminished. Ng et al. [29] found an increment in shear angle when the hardness of the job increased, while cutting forces were reduced when the hardness varied from 35 to 49 HRC.

At higher speed conditions (200 m/min), the resultant cutting force was leading when the workpiece hardness was growing from 28 to 42 HRC, while with a further increment in hardness, the resultant force was reduced.

Additionally, the turning parameters (cutting speed, feed, and depth of cut) had a notable impact on machinability measurement characteristics. The machining capability of the cutting tool was greatly affected by the turning parameters. The cutting tool had a higher machining life when the cutting speed was lower [30]. The tool may fail prematurely when the cutting speed was exceeded and induced greater stress (load) and temperature on the tip of the cutting tool. The higher feed induced higher friction during the cutting, and thus the cutting forces and roughness were increased. Many authors have stated that the cutting forces were prominently prejudiced by the tool feed speed and the depth of cut [31,32]. Kumar et al. [33,34] conducted hard turning experiments in dry, spray impingement cooling and nanofluid conditions. They noticed that the wear on the tool tip was impressively enhanced when the cutting speed was increasing. In addition, the surface roughness was prejudiced by the tool feed speed and the depth of cutting.

According to the literature review, many researchers have deliberated the machinability behaviors of AISI 4340 steel by using CVD as well as PVD-coated carbide tools. However, very few studies have reported the machinability behaviors of moderate hardness (30–40 HRC) AISI 4340 steel. The use of the PVD coated TiAlSiN carbide tool in turning AISI 4340 grade steel has yet to be reported in the open literature. In addition, the comparative machining capability of the CVD (TiCN-Al<sub>2</sub>O<sub>3</sub>-TiN) tool, PVD (TiAlN-TiN) tool, and PVD<sup>2</sup> (TiAlSiN) tool for hard material has not been studied yet. Additionally, Grey-Crow search hybrid optimization is a novel optimization tool and has not yet been implemented in any hard material machining. Based on these research gaps, this research presents an experimental investigation in hard turning AISI 4340 steel (30–40 HRC) by using three dissimilar carbide tools (CVD applied TiCN-Al<sub>2</sub>O<sub>3</sub>-TiN, PVD applied TiAlN-TiN, and PVD<sup>2</sup> applied TiAlSiN). The machining ability of these tools was compared based on measured cutting sound, power consumption, surface roughness, and cutting forces (radial, tangential, and feed). Moreover, a novel hybrid optimization (the Grey-Crow search algorithm) was implemented to estimate the optimal levels of input terms to compare the material removal rate of each tool for better sustainability.

## 2. Implementation Details

### 2.1. Details of the Workpiece

The test workpiece was taken as AISI 4340 steel having a cylindrical extruded diameter of 40 mm, while the original length was 250 mm. The chemical composition of the test workpiece was estimated using a thermo-scientific X-ray fluorescence spectrometer, and the results are shown in Table 1.

**Table 1.** Chemical composition of AISI 4340 alloy steel.

Elements	Fe	Cr	Ni	Mn	C	Mo	Si	Mg	P	Others
Content (% of weight)	95.17	1.58	1.48	0.59	0.35	0.19	0.18	0.05	0.02	0.39

### 2.2. Details of Cutting Inserts

The turning tests were accompanied using three distinct types of inserts: Tool-1: Walter CNMG-12s0408-NM4, Tool-2: TaeguTec DCMT11T308 MT TT5080, and Tool-3: Sumitomo electric WNMG080408N-GU. The details of the coatings and the geometry of each insert are listed in Table 2.

**Table 2.** Insert types and their geometries.

Tool			
	Tool-1	Tool-2	Tool-3
Brand	Walter	TaeguTec	Sumitomo
Code	CNMG-12s0408-NM4	DCMT11T308 MT TT5080	WNMG080408N-GU
Coatings	CVD (TiCN-Al <sub>2</sub> O <sub>3</sub> -TiN)	PVD (TiAlN-TiN)	PVD <sup>2</sup> (TiAlSiN)
Tool holder	TCLNL 25 25 M12 (MRK)	SDJCL 2525 M11 (Kennametal)	TWLNL 2525 M08 (AKKO)
Cutting edge length (mm)	12.9	10.8	8.69
Included angles	80°	55°	80°
Clearance angle	7°	7°	0°
Approach angle	95°	93°	95°
Orthogonal Rake angle	−6°	0°	−6°
Inclination angle	−6°	0°	−6°
Noise radius	0.8	0.8	0.8

### 2.3. Details of Surface Roughness Measurement

The average surface roughness ( $R_a$ ) of the test workpiece was obtained by a portable Mitutoyo SJ211 SurfTest instrument. The evaluation and cutoff lengths were taken as 4 mm and 0.8 mm, respectively. The roughness test was taken in the parallel direction of the axis of the machined workpiece, as displayed in Figure 1. The reading of  $R_a$  was noted at three different locations on the surface, and the mean value was evaluated. The average measurement error for  $R_a$  was found to be  $\pm 2.15\%$ .

**Figure 1.** Measuring setup of surface roughness tester and cutting sound.

#### 2.4. Details of Sound Measurement

Sound in this study is the total noise emitted by machine tools and the cutting process during the turning process. A Lutron SL-401 sound level meter was utilized to record the cutting sound. The sound measuring process was performed at the same point on the workpiece. The sound level meter was placed near the dead center of the CNC turning center, as shown in Figure 1. The average measurement error for the sound measurement was found to be  $\pm 1.31\%$ .

#### 2.5. Details of Cutting Force Measurement

The turning forces have been measured by a KISTLER 9129AA piezoelectric dynamometer. The three-directional turning force measurement was provided by a Kistler 3-component piezoelectric dynamometer that measures averaged tangential, feed, and radial forces during the turning processes. Graphical displays of force outputs are recorded using a data acquisition card (DAC) and Dynoware software at the end of each experiment. The average measurement error for forces  $F_x$ ,  $F_y$ , and  $F_z$  were found to be  $\pm 3.24\%$ ,  $\pm 2.68\%$ , and  $\pm 3.06\%$ , respectively. The experimental setup of force measurement is illustrated in Figure 2.

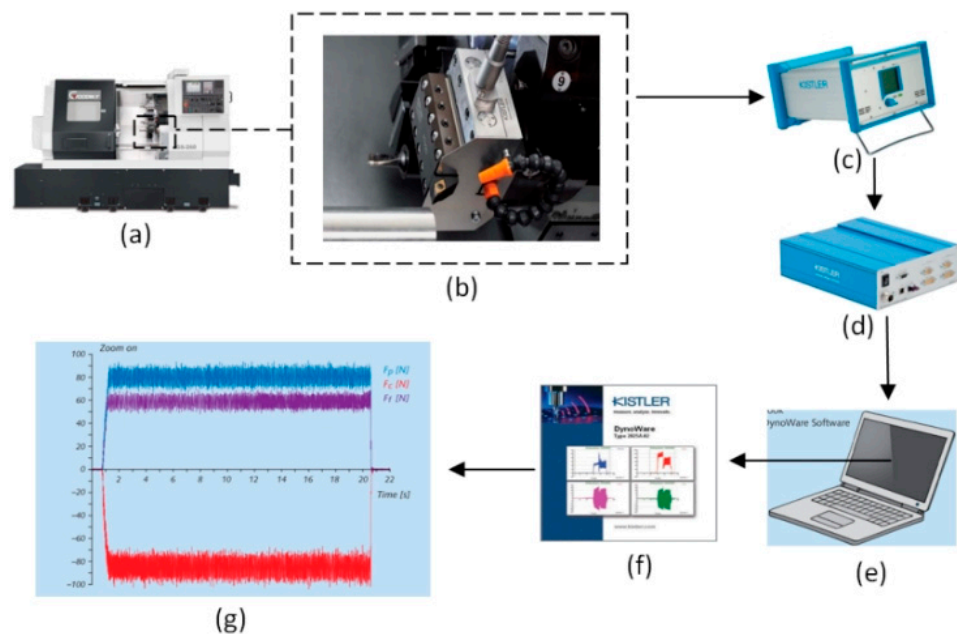


**Figure 2.** Cutting force measuring turning setup (a) CNC turning center, (b) Kistler piezoelectric dynamometer, (c) amplifier, (d) data acquisition system, (e) Computer, (f) Dynoware software, (g) force signals.

#### 2.6. Details of Cutting Power Measurement

In this study, the total power utilization in machining was estimated using the relation given in Equation (1) [35,36]. The required voltage (V) and Current (I) were measured using a UNI-T UT 201 Digital Clamp Multimeter. Furthermore, the power factor ( $\text{Cos}\theta$ ) was taken as 0.84 for a CNC lathe [35]. The average measurement error for cutting power was found to be  $\pm 1.76\%$ .

$$P = \sqrt{3} * V * I * \text{Cos}\theta \quad (1)$$

#### 2.7. Details of the Experimental Test

The turning tests were executed in dry surroundings using a Goodway GS-260Y model 5-axis CNC turning machine equipped with an extreme spindle speed of 4000 rpm and a motor of 15 kW. The turning tests were accomplished at three distinct cutting speeds (180, 220, and 260 m/min), feed rates (0.03, 0.07, and 0.11 mm/rev), depth of cuts

(0.08, 0.14, and 0.20 mm), three distinct hardness (30, 35, and 40 HRC), and three distinct cutting tools with different geometries and coatings (Table 1). The design of the experiments is used in many studies to establish the combination of the input parameters [37,38]. The experimental plan was executed using the Taguchi  $L_9$  design [39]. An  $L_9$  experiment for each type of insert was executed separately to compare their machining performances based on the results of three directional forces (Radial force  $F_x$ , Tangential force  $F_y$ , Feed force  $F_z$ ), surface roughness ( $R_a$ ), cutting sound ( $C_s$ ) and power consumption ( $P$ ). Furthermore, an analysis of variance (ANOVA) was used to determine the most effective input parameter on the responses [40,41]. For each turning test, a fresh edge of the tool was used to minimize the influence of the worn tool. The measurement of cutting forces, cutting sound, and electric current was accomplished during the cutting process, while the surface roughness was taken after the completion of each turning test. The electric current was utilized to estimate the cutting power. Furthermore, a novel hybrid optimization tool (grey-crow search algorithms) was applied to measure the optimal input variables for each tool. The entire research plan is schematically shown in Figure 3.

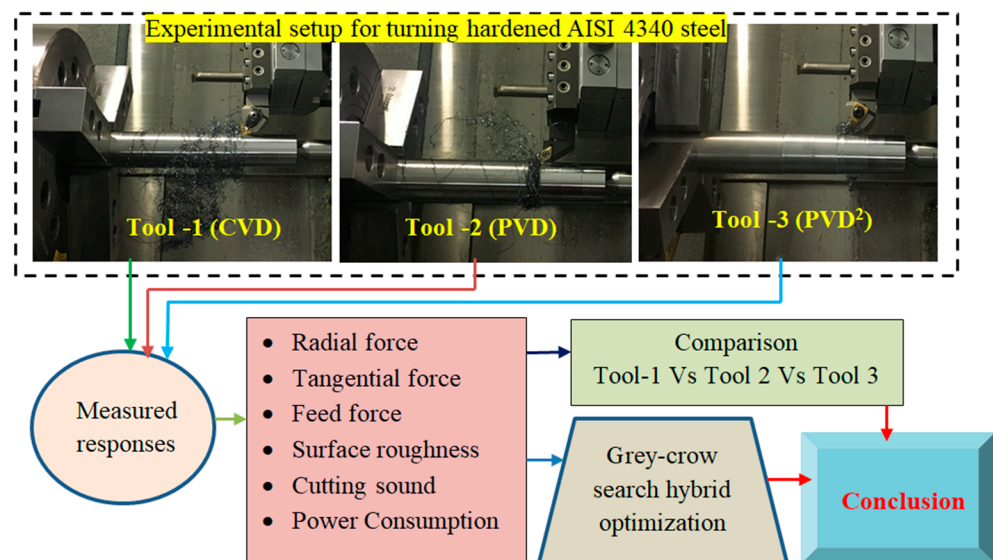


Figure 3. Overview of the research plan.

### 3. Results and Discussion

The turning tests were planned using a Taguchi  $L_9$  design, and the machinability indicator outputs ( $F_x$ ,  $F_y$ ,  $F_z$ ,  $R_a$ ,  $C_s$ , and  $P$ ) values are reported in Table 3.

**Table 3.** Turning test results.

Test No	Tool-1 (Walter CNMG-120408-NM4)									
	Input Values				Output Values					
	h (HRC)	V (m/min)	f (mm/rev)	a (mm)	F <sub>x</sub> (N)	F <sub>y</sub> (N)	F <sub>z</sub> (N)	R <sub>a</sub> (μm)	C <sub>s</sub> (dB)	P (kW)
1	30	180	0.03	0.08	55.11	33.69	47.83	0.33	79.9	3.324
2	30	220	0.07	0.14	106.50	64.44	71.74	0.48	84.6	3.605
3	30	260	0.11	0.20	142.70	102.3	89.61	0.63	89.6	3.917
4	35	180	0.07	0.20	93.31	72.70	56.87	0.74	80.5	3.367
5	35	220	0.11	0.08	91.83	48.61	40.84	0.62	84.9	3.326
6	35	260	0.03	0.14	66.61	30.45	39.26	0.53	89.7	3.887
7	40	180	0.11	0.14	103.30	61.73	45.61	0.82	80.7	3.101
8	40	220	0.03	0.20	67.50	35.72	48.34	0.73	87.7	3.619
9	40	260	0.07	0.08	78.26	35.26	37.24	0.64	89.0	3.738
	Tool-2 (TaeguTec DCMT11T308 MT TT5080)									
1	30	180	0.03	0.08	18.39	11.38	30.33	0.29	79.8	3.298
2	30	220	0.07	0.14	44.87	33.85	40.14	0.41	85.2	3.645
3	30	260	0.11	0.20	73.65	66.35	53.41	0.54	89.5	3.986
4	35	180	0.07	0.20	55.33	53.14	49.36	0.60	80.1	3.767
5	35	220	0.11	0.08	35.36	29.22	32.49	0.56	85.1	3.818
6	35	260	0.03	0.14	34.17	22.30	37.88	0.32	90.1	3.934
7	40	180	0.11	0.14	66.69	56.55	46.41	0.67	80.8	3.865
8	40	220	0.03	0.20	57.51	36.90	51.56	0.48	87.2	3.998
9	40	260	0.07	0.08	42.38	25.39	35.48	0.31	89.8	4.190
	Tool-3 (Sumitomo WNMG080408N-GU)									
1	30	180	0.03	0.08	12.97	11.44	30.6	0.27	79.1	2.985
2	30	220	0.07	0.14	35.11	33.77	39.79	0.40	83.5	3.516
3	30	260	0.11	0.20	60.57	68.48	53.43	0.51	89.2	4.065
4	35	180	0.07	0.20	39.67	40.58	44.24	0.39	79.4	3.195
5	35	220	0.11	0.08	25.44	22.00	31.88	0.48	83.5	3.342
6	35	260	0.03	0.14	22.52	14.77	35.73	0.19	89.9	3.775
7	40	180	0.11	0.14	47.80	44.90	42.63	0.47	79.8	3.022
8	40	220	0.03	0.20	36.97	26.05	44.52	0.26	86.1	3.365
9	40	260	0.07	0.08	24.98	19.56	32.09	0.30	88.2	3.665

### 3.1. Comparative Cutting Force Analysis

The assessment of cutting forces in the finished turning of the hardened steel was exploited to estimate the concert of the process in the chosen values of turning parameters. Here, all three components (radial-tangential-feed) of the turning force were measured for each tool. Overall, except for some test runs, the radial force for each tool was found to be greater in comparison to the other two components (tangential-feed) of the turning force. Many researchers have agreed that the radial directional force was superior to the tangential force, as well as the feed force in turning the hardened steel when the selected depth of the cut was less than the radii of the tool nose [42–44].

#### 3.1.1. Radial Force Analysis

The highest radial force for each tool was found when the turning was executed on the lowest hardness workpiece (30 HRC) at the highest magnitude of cutting speed (260 m/min), feed (0.11 mm/rev), and depth of cut (0.2 mm). This might be found due to a higher volume of metal removal in a single pass turning. Similarly, for each tool, the lowest radial force was achieved when turning was performed on a 30 HRC workpiece with the lowest level of all cutting parameters (first run for each tool). This might be due to the lower stock of material removal in single pass turning. From the comparative bar graph (Figure 4) and force signal images (Figure 5), the radial force for Tool-1 was traced to be the largest in comparison to Tool-2 and Tool-3 for each run. The least radial force was noticed for Tool-3, while the moderate radial force was achieved for Tool-2. In an average of all nine test results, Tool-1 was subjected to an 87.95% greater radial force relative to Tool-2, while it was 163.08% greater than Tool-3. Similarly, the radial for Tool-2 was 39.96% higher than for Tool-3. Considering the average results, the sequence of radial force for the tools was as follows: Tool-1 > Tool-2 > Tool-3. Therefore, as the radial force for Tool-1 was higher, more vibration and more tool deflection might have taken place as a result of the higher surface roughness in comparison to Tool-2 and Tool-3 (Table 3). In addition, it was found that the CVD coated (TiCN-Al<sub>2</sub>O<sub>3</sub>-TiN) tool was subjected to higher radial force in comparison to

the conventional PVD coated (TiAlN-TiN) and the second generation PVD (TiAlSiN) tools. TiAlSiN coating provided better resistance against the radial direction force, and as a result a better surface quality was obtained. Moreover, as a lower radial force was achieved with the TiAlSiN coated tool, it can be stated that more dimensional accuracy was achieved with this tool in comparison to the other tools.

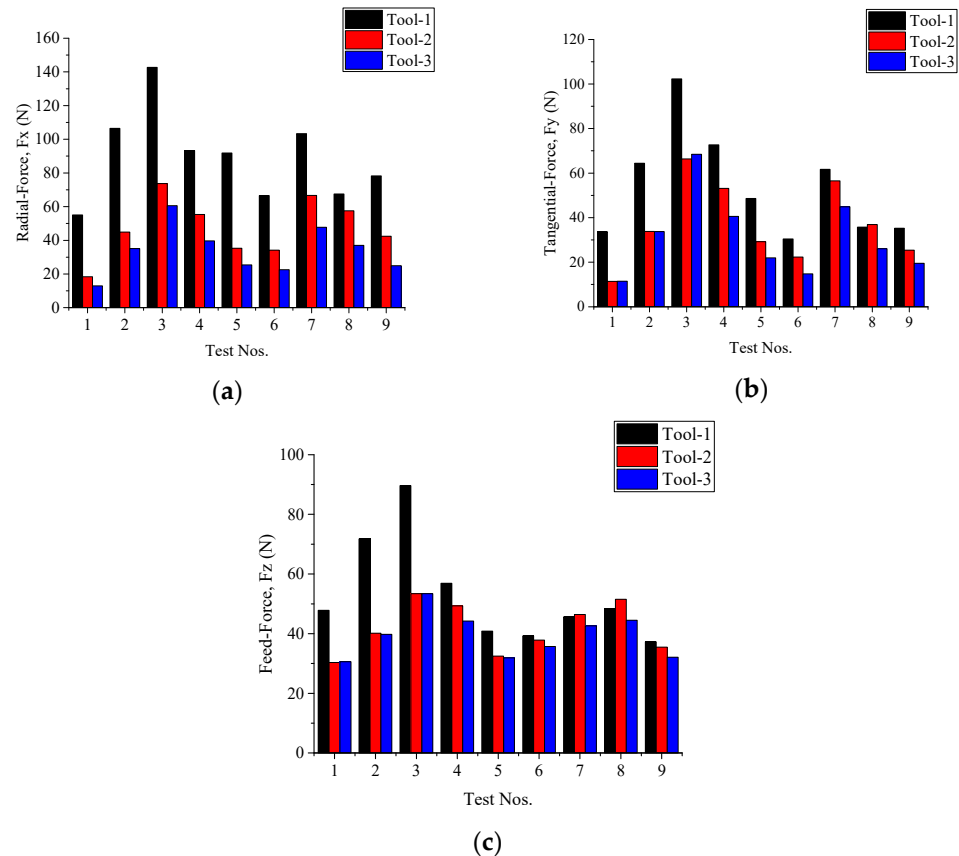


**Figure 4.** Comparison of forces for Tool-1, 2, and 3 (a) radial force, (b) tangential force, and (c) feed force.

For Tool-1 (the CVD tool),  $F_x$  was leading with rising feed, depth of cutting, and cutting speed, while it was deteriorating when the workpiece hardness was improving (Figure 6). The ANOVA results also confirmed the highest and most significant contribution of the feed (65.18%) towards affecting the  $F_x$  succeeded by the cutting depth (18.10%) and hardness of the workpiece (9.01%), while the effect of the cutting speed (3.79%) was not statically relevant ( $p > 0.05$ ). Aouici et al. [45] also stated that the cutting forces were considerably prejudiced by the cutting depth and hardness of the workpiece in turning hard AISI H11 grade steel. Similarly, for Tool-2 (PVD) and Tool-3 (2nd generation PVD), the  $F_x$  was leading with regard to improving the depth of cut and feed while with regard to the increment in workpiece hardness and cutting speed, the  $F_x$  was reducing from the first level to the second level of these parameters, while with the further increment in these parameters, the  $F_x$  was improving. The ANOVA (Table 4) also ensured the leading contribution of the depth of cut (52.76% for Tool-2 and 54.47% for Tool-3) followed by feed (29.67% for Tool-2 and 37.62% for Tool-3) towards  $F_x$ . Similarly, the terms (workpiece hardness and cutting speed) have an insignificant contribution towards  $F_x$  for Tool-2 and Tool-3. With regard to Bouziane et al. [46], the radial directional force was largely stimulated by the depth of cut (about 24.8%) and succeeded by the feed (about 10.2%) in turning the hardened bearing grade steels.

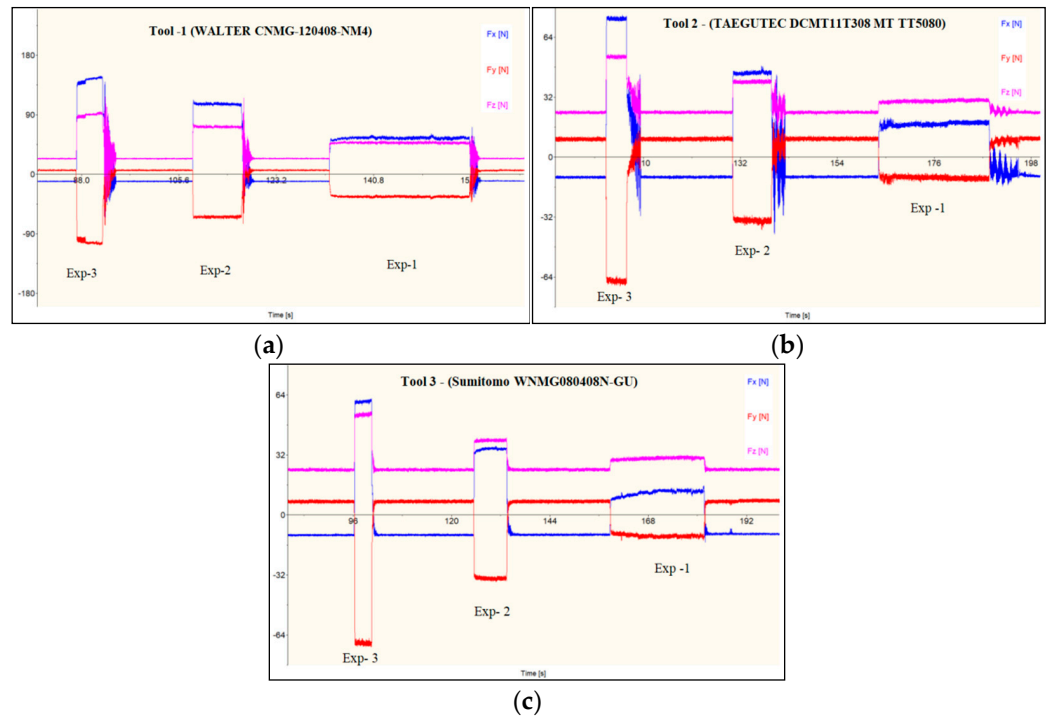


Figure 5. Force singles for experiments 1, 2, and 3 using (a) Tool-1, (b) Tool-2, and (c) Tool-3.

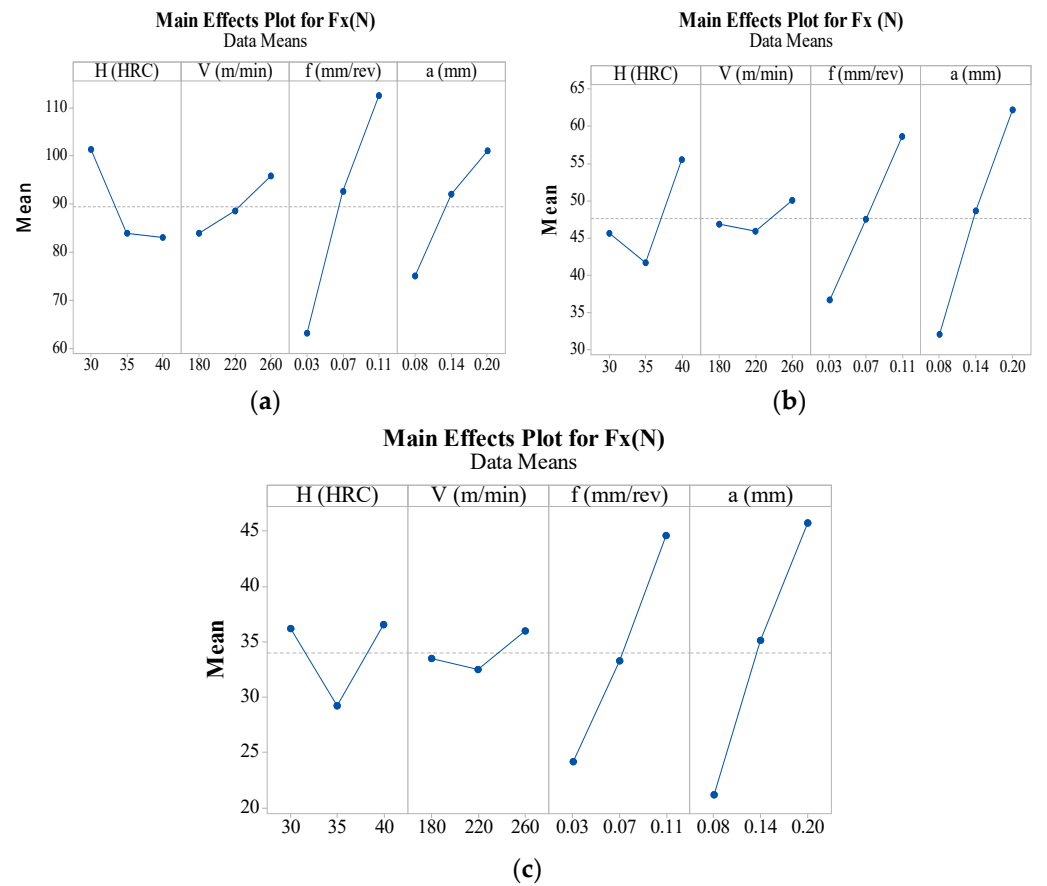


Figure 6. Effects of hardness and turning inputs on the radial force, Fx (a) Tool-1 (b) 2 and (c) 3.

**Table 4.** The estimation of the contribution of input terms (in %) on different forces using ANOVA.

Inputs	Tool-1			Tool-2			Tool-3		
	Fx	Fy	Fz	Fx	Fy	Fz	Fx	Fy	Fz
h (HRC)	<b>9.01</b>	<b>16.86</b>	<b>42.33</b>	6.06	0.34	2.61	0.01	3.47	0.76
V (m/min)	3.79	0.00	1.73	0.66	0.32	0.01	0.58	0.22	0.52
f (mm/rev)	<b>65.18</b>	<b>46.76</b>	11.49	<b>29.67</b>	<b>42.92</b>	4.48	<b>37.62</b>	<b>44.64</b>	10.63
a (mm)	<b>18.10</b>	<b>31.91</b>	<b>33.05</b>	<b>56.25</b>	<b>52.76</b>	<b>89.49</b>	<b>54.47</b>	<b>43.57</b>	<b>82.53</b>
<b>Significant/Insignificant at 95% of confidence level</b>									

### 3.1.2. Tangential Force Analysis

Similar to radial force analysis, for each tool, the highest and lowest magnitude of tangential force was noticed when turning was executed on 30 HRC workpieces at the highest (third run for each tool) and lowest (first run for each tool) levels of all turning parameters, respectively. In most of the tests, the magnitude of the tangential force for Tool-1 (CVD) was measured to be higher than that of Tool-2 (PVD) and Tool-3 (2nd generation PVD). In test run 8, the tangential force for Tool-2 was greater than Tool-1 and Tool-3, while in test no. 3, the tangential force for Tool-3 was measured to be greater than Tool-2. Therefore, except for test run 3, the tangential force for Tool-3 (TiAlSiN coated) was lower than for other tools. This may happen due to the better stable machining capability of the second generation PVD coated TiAlSiN cutting tool. In an average of all nine test results, Tool-1 was subjected to 44.71 % greater tangential force relative to Tool-2, while it was 72.22% greater than Tool-3. Similarly, the tangential force for Tool-2 was 19.01% higher than for Tool-3. Considering the average results, the sequence of tangential force for the tools was as follows: Tool-1 > Tool-2 > Tool-3.

The tangential force for Tool-1 was improved by increasing the magnitude of feed, depth of cutting, and workpiece hardness (Figure 7). Therefore, all of these terms are significant. According to the ANOVA report (Table 4), the highest stimulus on Fy was seen by feed (46.76%), followed by the depth of cutting (33.05%) and workpiece hardness (16.86%). The cutting speed had a negligible consequence on Fy, and thus was determined to be insignificant. Similarly, for Tool-2 and Tool-3, only the depth of cutting and feed seemed to be relevant, as Fy was leading with the cutting depth and tool feed. This might have happened due to the increasing cross-section of cut by the leading depth of the cut and feed. This consequence was agreed upon by many researchers [47]. For Tool-2, the depth of cutting has the largest impact on Fy, with a 52.76% contribution followed by the feed rate (42.92% impact). Similarly, for Tool-3, the feed has the largest impact on Fy, with a 44.64% impact, followed by the cutting depth (43.57% impact). Chinchankar and Choudhury [47] concluded that the cutting forces were principally prejudiced by the cutting depth (60–70%), and were followed by feed (25–30%) in machining the 4340 steel. In turning hard grade EN8 steel, Thangarasu et al. [48] found the largest impact (50.39%) of interaction terms (feed-depth of cut) on the cutting force while the individual factors (depth of cutting and feed) had a relevant stimulus on cutting force with the contribution of about 27.7% and 14.5%, respectively.

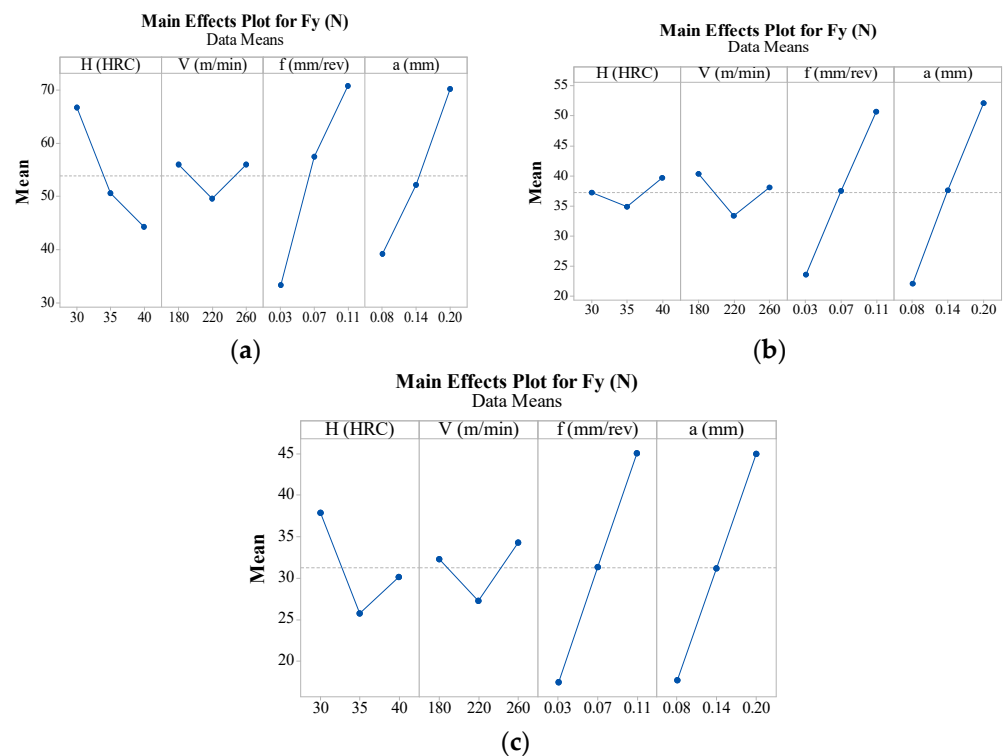


**Figure 7.** Effects of hardness and turning inputs on the tangential force,  $F_x$  (a) Tool-1 (b) 2 and (c) 3.

### 3.1.3. Feed Force Analysis

Similar to the radial as well as the tangential cutting force, the highest feed force for each tool was found when the turning test was executed on the lowest hardness workpiece (30 HRC) at the highest magnitude of cutting speed (260 m/min), feed (0.11 mm/rev), and depth of cut (0.2 mm). For Tool-1, the lowest feed force (37.24 N) was introduced when turning was performed on the highest workpiece hardness (40 HRC) using the highest speed (260 m/min), moderate feed (0.07 mm/rev), and the least cutting depth (0.08 mm). This might arise because of the lower thickness of material removal at the highest cutting speed. Similarly, for Tool-2 and Tool-3, the least feed force was noticed when the turning was accomplished on the least hardness of the workpiece (30 HRC) at low levels of cutting parameters. This might be the result of a lesser shear force requirement with regard to machining relatively lower hardness workpieces at the lowest feed and smallest cutting depth conditions. Overall, except for tests no 7 and 8, Tool-1 experienced a relatively greater feed force than Tool-2 and Tool-3. In tests no 7 and 8, Tool-2 had a relatively larger feed force than Tool-1 and Tool-3. In an average of all nine test results, Tool-1 was subjected to a 26.59% greater feed force relative to Tool-2, while it was 34.49% greater than for Tool-3. Similarly, the feed force for Tool-2 was 6.24% higher than it was for Tool-3. Considering the average results, the sequence of feed force for the tools was as follows: Tool-1 > Tool-2 > Tool-3.

Furthermore, the consequences of cutting terms on feed force were evaluated using the main effects plot (Figure 8) and ANOVA (Table 4). For Tool-1, the feed force ( $F_z$ ) was greatly reduced when the hardness of the workpiece was leading. This might have happened due to the leading cutting temperature and reduced contact area with increasing cutting speed. In addition,  $F_z$  was rising when the depth of the cutting, feed, and cutting speed was improving. Similarly, for Tool-2 and Tool-3, the force  $F_z$  was greatly increasing with the growing cutting depth, while it slowly increased with the gaining feed. It was also seen that the feed force was initially decreasing when the hardness was increased from 30 to 35 HRC; later on, with increasing hardness, it was enhanced. The marginal changes were seen in  $F_z$  when the cutting speed was leading. These assessments were greatly supported by the ANOVA results (Table 4). For Tool-1, the contribution of workpiece hardness was found to be 42.33%, followed by the depth of cutting (33.05%) and feed (11.49%). Statistically, the

terms cutting speed and feed were insignificant for  $F_z$ . For Tool-2 and Tool-3, only the depth of cut was significant, with contributions of 89.49% and 82.53% each. The remaining terms ( $h$ ,  $V$ , and  $f$ ) had an insignificant consequence on feed force. Referring to Bouziane et al. [46], in turning hard grade bearing steel, the feed directional force was largely stimulated by the cutting depth (about 26%), and was followed by the feed (about 4.4%).

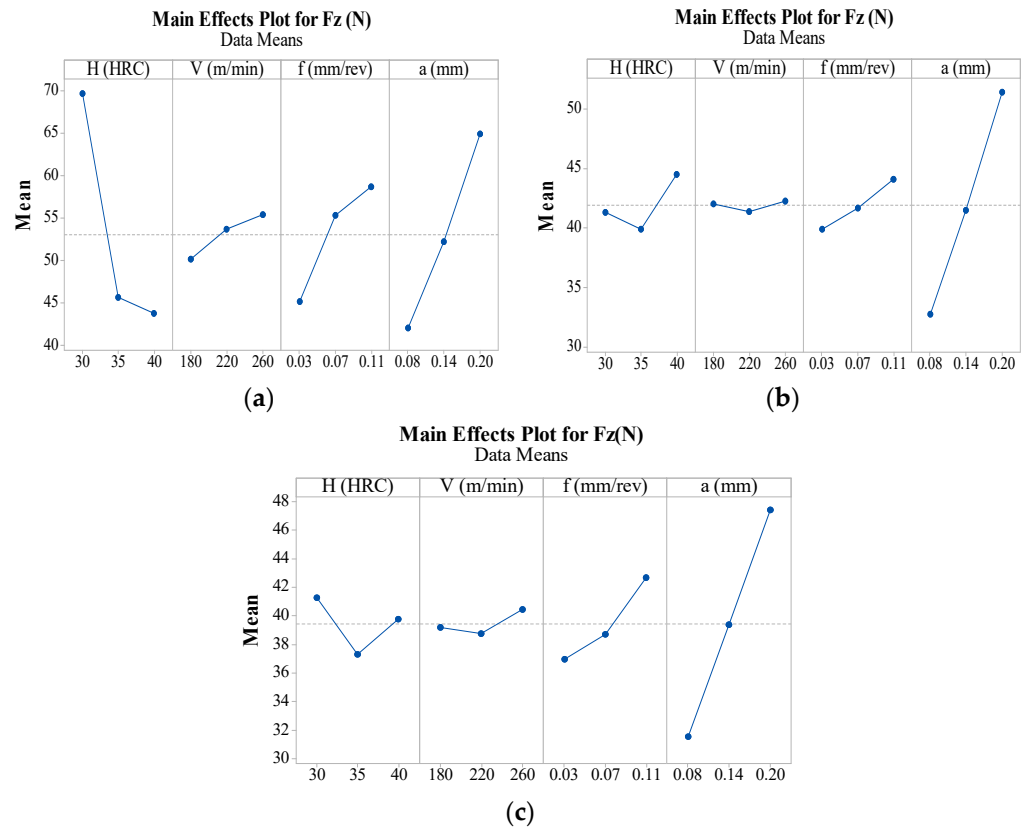


**Figure 8.** Effects of hardness and turning inputs on the feed force,  $F_x$ , (a) Tool-1, (b) 2, and (c) 3.

### 3.2. Comparative Surface Roughness Analysis

The desired surface quality is the prime concern for machinists with regard to their finished products remaining sellable in the competitive manufacturing world. The surface quality assessment in machinability was mainly based on the value of obtained surface roughness ( $R_a$ ) in any metal removing techniques. Therefore, in this study, the hard turning capability of the selected cutting tools was compared based on the experimentally obtained  $R_a$  values (Table 3). Furthermore, for better understanding, the  $R_a$  values for all tools were compared using a bar graph (Figure 9a). The maximum  $R_a$  in each test run was found when machining was executed with Tool-1. Tool-3 (the second generation TiAlSiN PVD coated tool) performed well and produced lesser  $R_a$  when compared to conventional PVD (Tool-2) and CVD (Tool-1) tools. According to Varghese [23], the superior wear resistance characteristics of the TiAlSiN coating tool were responsible for the improved surface finish. Sousa et al. [24] also specified that the TiAlSiN coating tool provided a much better surface finish than the TiAlN coating tool in hard milling due to the higher wear resistance capability and better surface finish of the TiAlSiN coating. In an average of all nine test  $R_a$  results, Tool-1 exhibited 32.05% greater roughness than Tool-2, while it exhibited 68.80% higher roughness than Tool-3. Similarly, Tool-2 exhibited 27.82% greater roughness compared to Tool 3. However, the sequence of the obtained  $R_a$  by different tools was as follows: Tool-1 > Tool-2 > Tool-3.

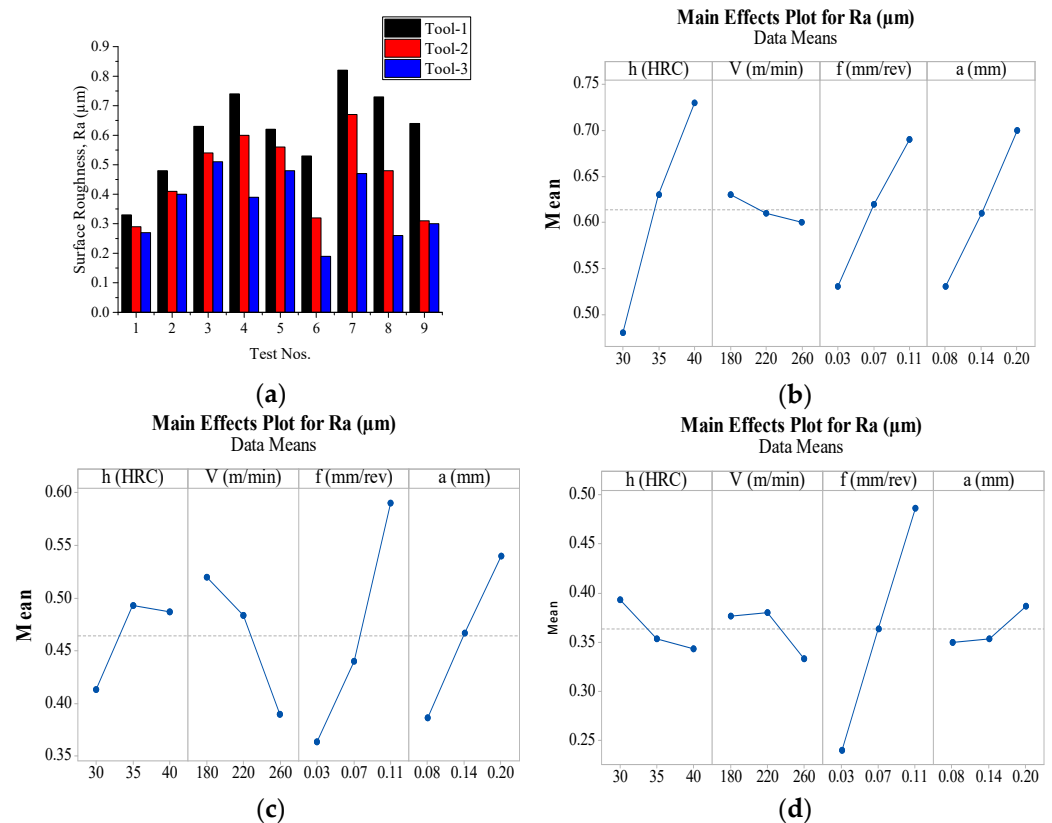


**Figure 9.** (a) Comparison of surface roughness among Tool-1, 2, and 3; (b–d) Effects of hardness and turning inputs on the surface roughness for Tool-1, 2, and 3, respectively.

Moreover, the consequence of cutting terms on Ra was addressed using main effects plots (Figure 9b–d) and an ANOVA (Table 5). The Ra (Tool-1) improved with the leading value of workpiece hardness, feed, and cutting depth, while it deteriorated with increasing speed. Bhuiyan and Choudhury [49] also reported an increment in roughness with leading workpiece hardness. Ozel et al. [50] reported the marginal increment in Ra when the job hardness was increased from 51.3 to 54.7 HRC in turning hard AISI H13 steel, while Ra was greatly stimulated by the feed rate. The ANOVA (Table 5) also disclosed that the surface roughness was greatly altered by workpiece hardness (52.55%), and lagged by the cutting depth (24.52%) and feed (21.52%). The ANOVA report also confirmed the significant stimulus of these terms on Ra, while the cutting speed was insignificant. Chinchankar and Choudhury [47] also found a significant consequence of workpiece hardness, feed, and cutting depth on the obtained surface roughness in turning hard AISI 4340 grade steel. Similarly, for Tool-2, the surface roughness was increasing with the rising feed and cutting depth. In addition, the roughness was leading when the job hardness was changing from 30 HRC to 35 HRC, while with an additional increment in hardness, the roughness was slightly reduced. The Ra value was deteriorating with the leading speed. The ANOVA (Table 5) ensured that the feed and cutting depth had an important consequence on Ra, with a contribution of 50.10% and 22.92%, respectively, while other terms had insignificant contributions. D’addona and Raykar [51] revealed that the Ra was greatly exaggerated by the feed dawdled by the cutting depth and the type of insert in the hard turning of 55 HRC steel. In addition, Bag et al. [52] also found the uppermost consequence of feed rate on Ra (71.9%), followed by speed (14.7%) and cutting depth (3.4%) in hard turning on AISI 4340 steel using an  $\text{Al}_2\text{O}_3$  top layer coated CVD tool. For Tool-3, the Ra was linearly raised with the leading feed, while other terms had a marginal consequence on Ra. The ANOVA (Table 5) also indicated that feed was the only significant term, with an 89.47% contribution, while the other terms were insignificant.

**Table 5.** Estimation of contribution of input terms (in %) on Ra, Cs, and P using ANOVA.

Inputs	Tool-1			Tool-2			Tool-3		
	Ra	Cs	P	Ra	Cs	P	Ra	Cs	P
h (HRC)	52.55	1.38	4.00	5.24	1.27	40.84	3.67	0.60	4.33
V (m/min)	0.75	94.00	81.37	16.48	96.58	45.02	2.76	95.74	86.99
f (mm/rev)	21.52	0.56	6.27	50.10	0.51	6.23	89.47	0.76	1.51
a (mm)	24.29	2.03	7.04	22.92	1.28	6.40	2.10	1.15	6.57
Significant/Insignificant based on 95% of confidence level									

### 3.3. Comparative Cutting Sound Analysis

In the metal cutting industry, the cutting sound is considered to be an important health issue for individuals who are working around machining activities. This unpleasant sound had a significant influence on the hearing of the operators, as they spent at least 8 h per day in this noisy environment [53]. Therefore, to achieve sustainable machining, the cutting sound must be controlled to avoid damage to the hearing of workers present during that process. However, in this research, the cutting sound for each type of tool was measured in turning 4340 hardened steel.

The range of measured cutting sound for Tool-1, Tool-2, and Tool-3 was found as (79.7–89.7 dB), (79.8–90.1 dB), and (79.1–89.9 dB), respectively (Table 3). In an average of all nine test results, the average cutting sound generated for Tool-1, Tool-2, and Tool-3 was 85.17 dB, 85.28 dB, and 84.30 dB, respectively. Therefore, turning with Tool-3 exhibited relatively lesser cutting sound than Tool-1 and Tool-2 (Figure 10a). The highest cutting sound for each tool was emitted when turning was executed on the moderate hardness of the job (35 HRC), with a maximum speed (260 m/min), least feed (0.03 mm/rev), and moderate cutting depth (0.14 mm). Similarly, the least cutting sound for each tool evolved when the test was performed on the lowest hardness job (30 HRC), with the least values of speed, feed, and cutting depth.

The effects of work hardness and turning parameters on the cutting sound were investigated using main effects pots (Figure 10b–d) and an ANOVA (Table 5). For each tool, the cutting sound was rapidly enhanced with increasing speed due to the vibration and speed involved in hard turning. As indicated in many studies [53,54], the sound generation from machining was very sensitive to changes in the cutting speed. Many researchers agreed that the cutting sound was leading to an increasing cutting speed [55–57]. The effect of work hardness was marginal, but the cutting sound was enhanced slowly with the leading hardness of the job. Similarly, there were negligible effects of feed as well as cutting depth on the cutting sound. The marginal enhancement in cutting sound was seen with the leading depth of cut. The ANOVA (Table 5) indicated that the cutting speed was the only significant factor for cutting sound, while the other terms were insignificant. The contribution of cutting speed towards the cutting sound for Tool-1, Tool-2, and Tool-3 was estimated as 94.00%, 96.58%, and 86.99%, respectively.

### 3.4. Comparative Power Consumption Analysis

In metal machining, electricity consumption plays a significant role in the overall machining cost. According to the report of the International Energy Agency in 2009, electricity utilization is expected to improve by about 1.5% yearly from 2007 to 2030, and an enormous amount of it will be used by China and India. In fact, in another report, it was mentioned that electricity consumption in the US alone would increase by 50% by the year 2030 [58,59]. Furthermore, power consumption is one of the essential elements that stimulates the attainability of sustainable hard machining. Therefore, minimal power consumption is desirable for hard machining, and many researchers have tried to implement various machining attributes in hard machining to achieve it.

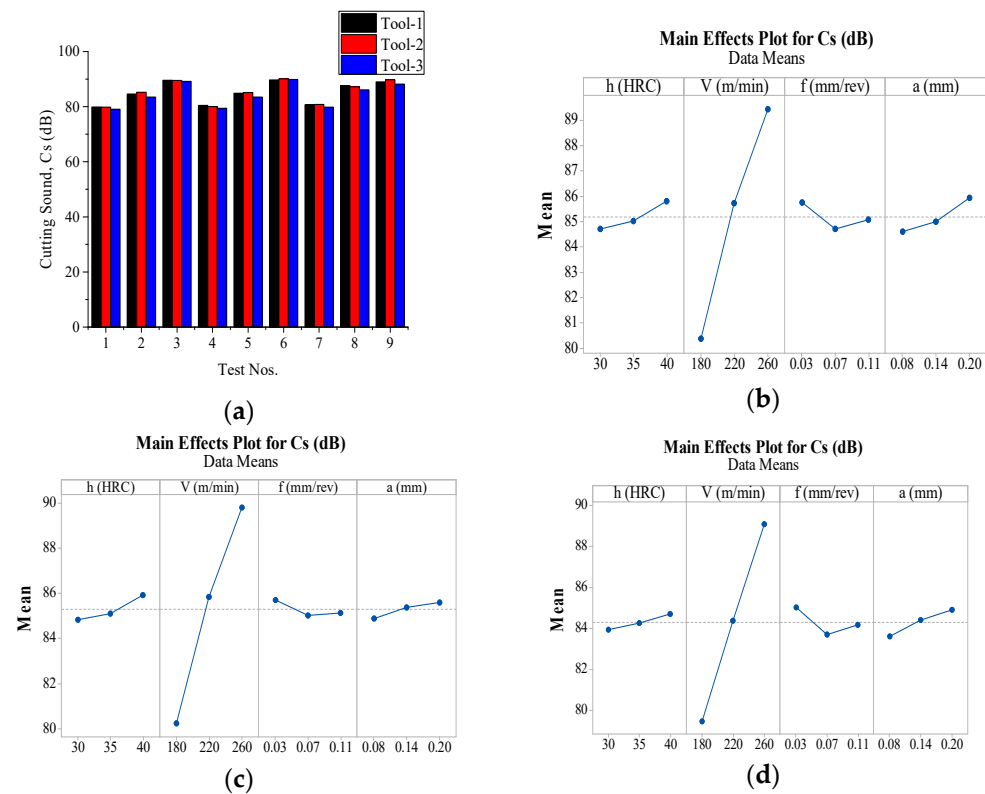


**Figure 10.** (a) Comparison of the cutting sound among Tool-1, 2, and 3 (b–d) Effects of hardness and turning inputs parameters on cutting sound for Tool-1, 2, and 3, respectively.

According to the estimated power results (Figure 11a), except for test nos. 1 and 3, the power utilization in machining with Tool-2 was determined to be greater than for the other tools. In an average of all nine experiments, Tool-2 had 8.2% higher power utilization than Tool-1, while it had 11.54% higher power utilization than Tool-3. In comparison with Tool-1 and Tool-3, Tool-2 had 3.08% higher power consumption than Tool-3. Therefore, it can be stated that Tool-3 had the least power consumption in comparison to other tools due to the least friction coefficient of the TiAlSiN coating surface with regard to the TiAlN (Tool-2) and TiN (Tool-1) surface. The lowest friction coefficient of the TiAlSiN coated tool enables the least cutting friction and cutting force in machining hardened steel among the TiAlN coated and TiN coated tools, and as a result lower power consumption was achieved with the TiAlSiN-coated tool.

Additionally, the impact of the cutting terms was assessed using the main effects plot (Figure 11b–d) and the ANOVA (Table 5). For Tool-1 and Tool-3, the power consumption was leading with cutting speed, while other parameters had little influence on power consumption. For Tool-2, power consumption was leading, with workpiece hardness, speed, feed, and depth of cutting, but the effects of workpiece hardness and speed were dominant. According to the ANOVA (Table 5), cutting speed was the only relevant factor for power consumption with a percentage of contribution of (81.37%) and (86.99%) for Tool-1 and Tool-3, respectively, while the hardness of the workpiece and speed were the relevant terms for Tool-2, with a percentage of contribution of (40.84%) and (45.02%), respectively. Şahinoglu and Rafighi [14] reported that the feed and cutting depth affected the cutting power greatly in machining AISI 1040 steel.

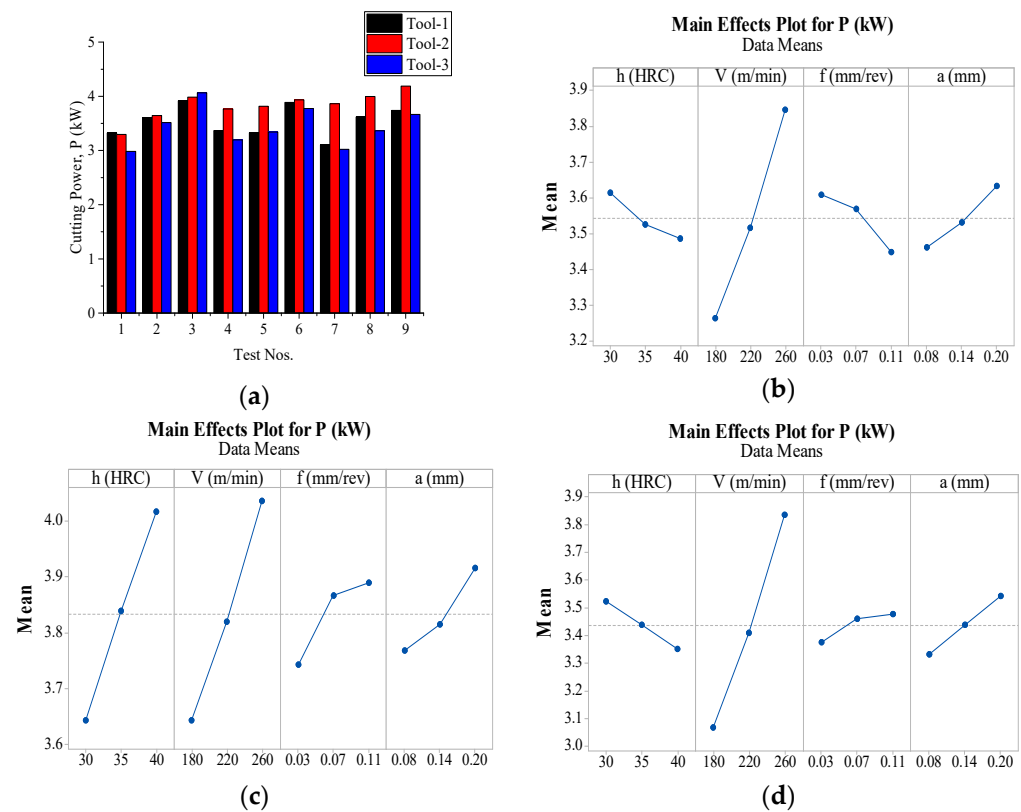


**Figure 11.** (a) Comparison of power consumption among Tool-1, 2, and 3; (b–d) Effects of hardness and turning inputs on the power consumption of Tool-1, 2, and 3, respectively.

#### 4. Grey-Crow Search Hybrid Optimization

A recent trend has seen the concept of hybrid optimization successfully implemented in hard machining. In this hybrid mode, the concepts of conventional optimization and advanced algorithm were coupled and implemented for optimizing the machining attributes. In the current research, the grey relational analysis optimization tool was coupled with the crow search algorithm and was utilized to optimize the hard turning input parameters for each type of cutting tool. The step-wise procedure of this hybrid methodology is shown in Figure 12.

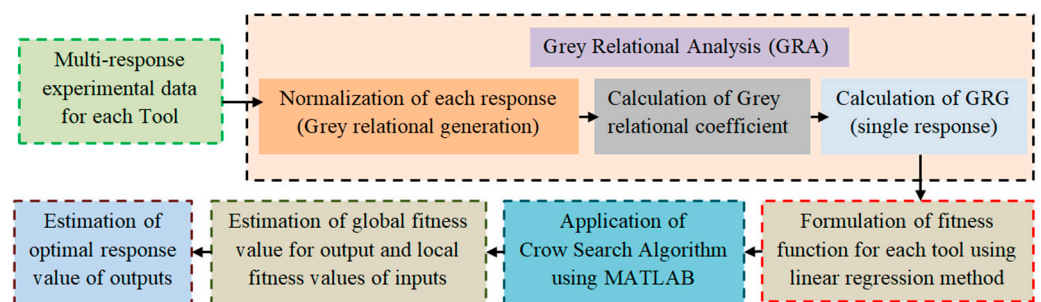


**Figure 12.** Steps of grey-crow search hybrid optimization.

In this methodology, each response data point was initially normalized using Equation (2) [30], and the normalized value for each response is displayed in Table 6. The normalized data also allowed for grey relational generation. In the next step, the grey relational coefficient was calculated using Equation (3) [30], and is shown in Table 6.

$$N_i(k) = \frac{Max\{N_i(k)\} - N_i(k)}{Max\{N_i(k)\} - Min\{N_i(k)\}} \tag{2}$$

where,  $N_i(k)$  symbolizes the normalized value (grey relational generation).  $Max\{N_i(k)\}$  and  $Min\{N_i(k)\}$  denote the biggest and least value of  $N_i(k)$ , respectively for the  $k$ th response.

$$M_i(k) = \frac{\Delta_{Min} + \omega \cdot \Delta_{Max}}{\Delta_{0i}(k) + \omega \cdot \Delta_{Max}} \tag{3}$$

where,  $\Delta_{0i}(k) = \|M_0(k) - M_i(k)\|$  is the estimated difference value between ‘ $M_0(k)$ ’ and ‘ $M_i(k)$ ’. ‘ $\omega$ ’ is the distinguishing coefficient that varied between 0 to 1 [30]. In the current analysis, it was taken as 0.5. ‘ $\Delta_{Min}$ ’ and ‘ $\Delta_{Max}$ ’ are the minimal and maximum values calculated ‘ $\Delta_{0i}(k)$ ’.

**Table 6.** Estimation of GRG.

Test No.	Grey Relation Generation						Grey Relation Coefficient						GRG
	Fx	Fy	Fz	Ra	Cs	P	Fx	Fy	Fz	Ra	Cs	P	
Tool-1 (WALTER CNMG-120408-NM4)													
1	1.000	0.955	0.798	1.000	1.000	0.727	1.000	0.917	0.712	1.000	1.000	0.647	<b>0.879</b>
2	0.413	0.527	0.341	0.694	0.520	0.382	0.460	0.514	0.431	0.620	0.510	0.447	0.497
3	0.000	0.000	0.000	0.388	0.010	0.000	0.333	0.333	0.333	0.450	0.336	0.333	0.353
4	0.564	0.412	0.625	0.163	0.939	0.674	0.534	0.460	0.572	0.374	0.891	0.605	0.573
5	0.581	0.747	0.931	0.408	0.490	0.724	0.544	0.664	0.879	0.458	0.495	0.645	0.614
6	0.869	1.000	0.961	0.592	0.000	0.037	0.792	1.000	0.928	0.551	0.333	0.342	0.658
7	0.450	0.565	0.840	0.000	0.918	1.000	0.476	0.535	0.758	0.333	0.860	1.000	0.660
8	0.859	0.927	0.788	0.184	0.204	0.365	0.779	0.872	0.702	0.380	0.386	0.441	0.593
9	0.736	0.933	1.000	0.367	0.071	0.219	0.654	0.882	1.000	0.441	0.350	0.390	0.620
Tool-2 (TAEGUTEC DCMT11T308 MT TT5080)													
1	1.000	1.000	1.000	1.000	1.000	1.000	1.000	1.000	1.000	1.000	1.000	1.000	<b>1.000</b>
2	0.521	0.591	0.575	0.684	0.476	0.611	0.511	0.550	0.541	0.613	0.488	0.562	0.544
3	0.000	0.000	0.000	0.342	0.058	0.229	0.333	0.333	0.333	0.432	0.347	0.393	0.362
4	0.332	0.240	0.175	0.184	0.971	0.474	0.428	0.397	0.377	0.380	0.945	0.487	0.502
5	0.693	0.675	0.906	0.289	0.485	0.417	0.620	0.606	0.842	0.413	0.493	0.462	0.573
6	0.714	0.801	0.673	0.921	0.000	0.287	0.636	0.716	0.605	0.864	0.333	0.412	0.594
7	0.126	0.178	0.303	0.000	0.903	0.364	0.364	0.378	0.418	0.333	0.837	0.440	0.462
8	0.292	0.536	0.080	0.500	0.282	0.215	0.414	0.519	0.352	0.500	0.410	0.389	0.431
9	0.566	0.745	0.777	0.947	0.029	0.000	0.535	0.662	0.691	0.905	0.340	0.333	0.578
Tool-3 (Sumitomo WNMG080408N-GU)													
1	1.000	1.000	1.000	0.750	1.000	1.000	1.000	1.000	1.000	0.667	1.000	1.000	<b>0.944</b>
2	0.535	0.609	0.597	0.344	0.593	0.508	0.518	0.561	0.554	0.432	0.551	0.504	0.520
3	0.000	0.000	0.000	0.000	0.065	0.000	0.333	0.333	0.333	0.333	0.348	0.333	0.336
4	0.439	0.489	0.403	0.375	0.972	0.806	0.471	0.495	0.456	0.444	0.947	0.720	0.589
5	0.738	0.815	0.944	0.094	0.593	0.669	0.656	0.730	0.899	0.356	0.551	0.602	0.632
6	0.799	0.942	0.775	1.000	0.000	0.269	0.714	0.895	0.690	1.000	0.333	0.406	0.673
7	0.268	0.413	0.473	0.125	0.935	0.966	0.406	0.460	0.487	0.364	0.885	0.936	0.590
8	0.496	0.744	0.390	0.781	0.352	0.648	0.498	0.661	0.451	0.696	0.435	0.587	0.555
9	0.748	0.858	0.935	0.656	0.157	0.370	0.665	0.778	0.885	0.593	0.372	0.443	0.623

In the coming step, the grey relational grade (GRG) was estimated based on Equation (4), and is mentioned in Table 6 for all three types of tools.

$$\beta_i = \frac{1}{j} \sum_{k=1}^j M_i(k) \tag{4}$$

where, ‘ $j$ ’ denotes the number of responses studied.

However, with the help of grey relational analysis, the multi-responses are now transformed into a single response as GRG. In the next step, using the GRG as an output and all four input variables, a linear regression model was developed for each tool. These models will be used as a fitness function for the Crow search algorithm (CSA) in order to explore the optimum best values for various machining terms. The developed fitness function for Tool-1, Tool-2, and Tool-3 was noted in Equations (5)–(7) individually.

$$GRG (Tool-1) = 1.257 + (0.00479 \times h) - (0.002007 \times V) - (2.096 \times f) - (1.650 \times a) \quad (5)$$

$$GRG (Tool-2) = 1.979 - (0.01453 \times h) - (0.001792 \times V) - (2.619 \times f) - (2.376 \times a) \quad (6)$$

$$GRG (Tool-3) = 1.556 - (0.00112 \times h) - (0.002048 \times V) - (2.560 \times f) - (2.000 \times a) \quad (7)$$

Crow Search Algorithm (CSA) is a population-related stochastic algorithm stimulated by the intelligent behavior of crows. This algorithm works based on the excess food storing behavior of crows, in which the crows hide the extra amount of food, and the food is retrieved when the crows need it. Askarzadeh [60] developed the CSA algorithm in the year 2016. The author has implemented the developed algorithm to optimize the different parameters of engineering design problems, and the acquired outcomes were equated with the outcomes of other well-known optimization algorithms such as the Genetic Algorithm (GA), Particle Swarm Optimization (PSO), and Harmony Search (HS). The comparative analysis indicated that the CSA provided better-optimized values for engineering design parameters than the other optimization algorithms. Therefore, the present work selects and implements the CSA to find the optimal or near-optimal value for different machine parameters for all three tools.

In CSA, the number of crows ( $n$ ) is first initialized in the search domain ( $d$ ). After that, it is presumed that  $i$  is the position of the crow at iteration ( $it$ ) in the search domain, which is demarcated by the vector  $V^{i,it} = [V_1^{i,it}, V_2^{i,it}, \dots, V_d^{i,it}]$  where  $i = 1, 2, 3, \dots, n$  and  $it = 1, 2, 3, \dots, it_{max}$ ;  $it_{max}$  represents the defined maximum number of iterations. Assume that each crow has a memory, and the position of the hiding place is stored in that memory. The location of the hiding place of  $i$ -crow at any iteration is memorized as  $m^{i,it}$ . Suppose that at any iteration, the second crow  $j$  wants to go to its hiding location defined by  $m^{j,it}$ . At the same iteration, the first crow  $i$  thinks to follow the second crow  $j$  to see the hiding place of the second crow  $j$ . The following two cases may result given this condition:

Case 1: The second crow  $j$  is not aware that the first crow  $i$  is following it. In this condition, the first crow  $i$  will try to reach the hiding position of the second crow  $j$ , and the new position of the first crow  $i$  is calculated using Equation (8).

$$V^{i,it+1} = V^{i,it} + r_i \cdot fl^{i,it} \cdot (m^{j,iter} - V^{i,it}) \quad (8)$$

where,  $r_i$  is a random number vector and lies between  $[0 \ 1]$  in the algorithm.  $fl^{i,it}$  defines the flight length of the 1st crow  $i$  at iteration ( $it$ ).

Case 2: The second crow  $j$  knows the first crow  $i$  is following it. In this condition, the second crow  $j$  will try to defend its hidden food from being stolen, and the second crow  $j$  will fool the first crow  $i$  by going to another position in the search domain. Both cases may be represented, as shown in Equation (9):

$$V^{i,it+1} = \begin{cases} V^{i,it} + r_i \cdot fl^{i,it} \cdot (m^{j,iter} - V^{i,it}) & \text{when } r_j \geq AP^{i,it} \\ \text{a random position} & \text{otherwise} \end{cases} \quad (9)$$

where  $r_j$  a random number is a vector and lies between  $[0 \ 1]$  in the algorithm.  $AP^{i,it}$  signifies the responsiveness probability of the second crow  $j$  at iteration ( $it$ ).

Figure 13 reveals the generalized flowchart of a Crow Search Algorithm (CSA). It is implemented in the present work to get the local and global optimum machine parameters

of the input (independent) and output (dependent) variables for Tool-1, Tool-2, and Tool-3. The best fitness values of GRG for Tool-1, Tool-2, and Tool-3 can be seen in Figure 14a–c, respectively, which are received after the completion of 1000 iterations in the CSA.

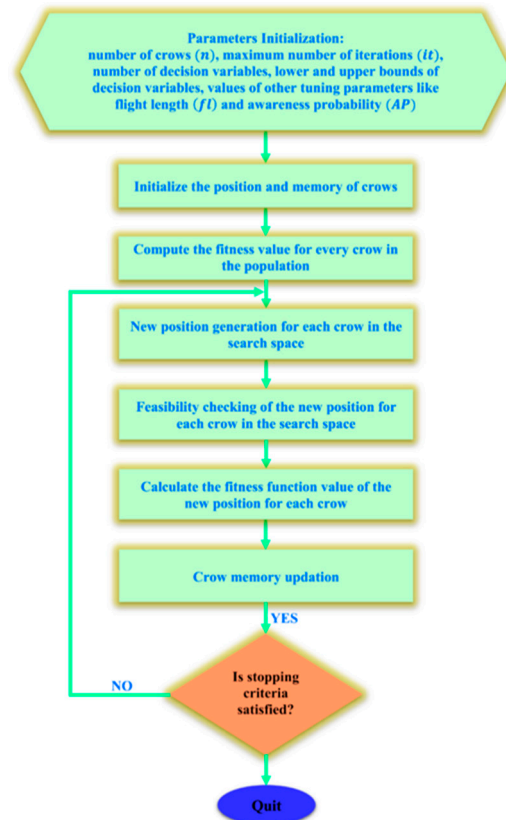


**Figure 13.** Generalized flowchart of a Crow Search Algorithm (CSA).

For Tool-1, the best fitness value of GRG was found to be 0.88559, which shows that the following local optimum machine parameters of the input variables are:  $h = 30$  HRC,  $V = 182$  m/min,  $f = 0.04$  mm/rev, and  $a = 0.0879$  mm, and their corresponding global optimum machine parameters of the output (dependent) variables are:  $F_x = 63.081$  N,  $F_y = 37.603$  N,  $F_z = 48.484$  N,  $R_a = 0.369$   $\mu\text{m}$ ,  $C_s = 80.005$  dB, and  $p = 3.317$  kW. Similarly, for Tool-2, the best fitness value of GRG is 0.9881, which reveals that the following local optimum machine parameters of the input variables are:  $h = 32$  HRC,  $V = 182$  m/min,  $f = 0.04$  mm/rev, and  $a = 0.0833$  mm, and their corresponding global optimum machine parameters of the output (dependent) variables are:  $F_x = 20.642$  N,  $F_y = 13.188$  N,  $F_z = 30.440$  N,  $R_a = 0.347$   $\mu\text{m}$ ,  $C_s = 80.296$  dB, and  $p = 3.409$  kW. Finally, for Tool-3, the best fitness value of GRG is found to be 0.8872, which reveals that the following local optimum machine parameters of the input variables are:  $h = 32$  HRC,  $V = 220$  m/min,  $f = 0.04$  mm/rev, and  $a = 0.0865$  mm, and their corresponding global optimum machine parameters of the output (dependent) variables are:  $F_x = 15.246$  N,  $F_y = 10.998$  N,  $F_z = 30.674$  N,  $R_a = 0.269$   $\mu\text{m}$ ,  $C_s = 83.815$  dB, and  $p = 3.356$  kW. Furthermore, using the optimal input parameter values of each tool, the material removal rate (MRR) for one pass was calculated using the theoretical formula ( $MRR = Vfa$ ). The MRR for Tool-1 (with job hardness 30 HRC), Tool-2 (with job hardness 32 HRC), and Tool-3 (with job hardness 32 HRC) were found to be 639.9, 606.4, and 761.2  $\text{mm}^3/\text{min}$ , respectively. Therefore, Tool-3 has a more preferable MRR in comparison to Tool-2 and Tool-1.

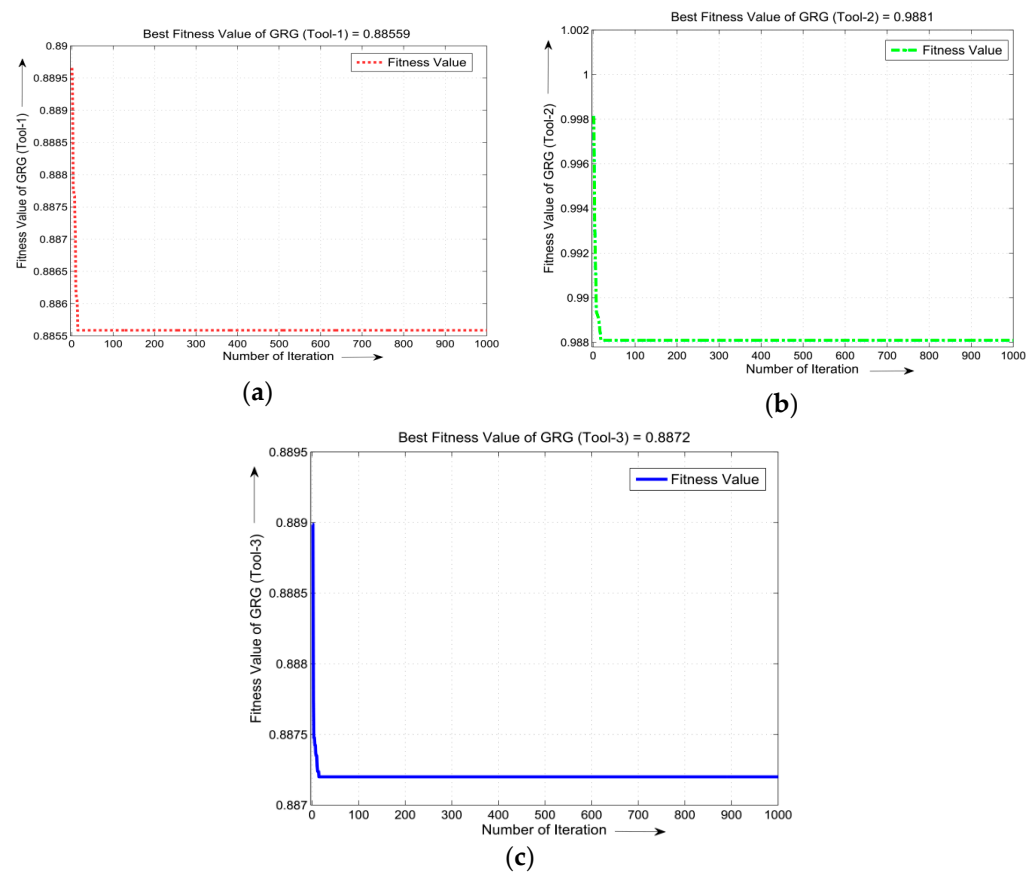


**Figure 14.** Fitness function plot of best fitness value of GRG and the number of iterations for (a) Tool-1; (b) Tool-2; and (c) Tool-3.

## 5. Conclusions

This research elaborates on the machining performance of Tool-1 (CVD applied TiCN- $\text{Al}_2\text{O}_3$ -TiN coatings), Tool-2 (PVD applied TiAlN-TiN coatings), and Tool-3 (PVD<sup>2</sup> applied TiAlSiN coatings) carbide inserts in turning hardened AISI 4340 steel. The performances of the cutting inserts were compared considering the results of the cutting sound, power consumption, surface roughness, radial force, tangential force, and feed force. Additionally, a novel hybrid optimization approach, namely the grey-crow search algorithm, was implemented to find the optimal turning parameter level for these inserts. The following major conclusions were reached:

- Considering the average results, the sequence of each component of cutting forces for the tools was as follows: Tool-1 > Tool-2 > Tool-3. A similar sequence was obtained for surface roughness, cutting sound, and power consumption.
- For the radial force, the feed rate was the most dominant input for Tool-1 (65.18%), while for Tool-2 and Tool-3, the most significant input was depth of cut, with a contribution of 56.25% and 54.47%, respectively.
- For the tangential force, the feed rate was observed to be the most noteworthy input for Tool-1 (46.76%) and Tool-3 (44.64%), while the depth of cut (52.76%) was the largest significant term for Tool-2.
- For the feed force, the workpiece hardness (42.33%) was the primary dominating character for Tool-1, while for Tool-2 and Tool-3, the depth of cut was determined to be the most influential contributor, at 89.49% and 82.53%, respectively.
- The acceptable range of surface quality (1.6  $\mu\text{m}$ ) was observed for each tool. The variations in Ra value for Tool-1, Tool-2, and Tool-3 were found to be (0.33–0.82  $\mu\text{m}$ ), (0.29–0.67  $\mu\text{m}$ ), and (0.19–0.51  $\mu\text{m}$ ). Therefore, Tool-3 provided the best finishing quality among all tools.

- The cutting speed was the primary factor in the cutting sound in hard turning. The contribution of cutting speed for Tool-1, Tool-2, and Tool-3 was found to be 94.00%, 96.58%, and 95.74%, respectively.
- Tool 3 has the lowest power consumption relative to the other tools due to having the lowest frictional coefficient of TiAlSiN coating applied on Tool-3. As a result, lower cutting forces and thus a lower power consumption in the machining hardened steel was realized.
- The optimum levels of input terms were obtained using a grey-crow search algorithm hybrid optimization. The optimal levels for Tool-1 were found to be  $h = 30$  HRC,  $V = 182$  m/min,  $f = 0.04$  mm/rev, and  $a = 0.0879$  mm; similarly, for Tool-2, the optimal levels were  $h = 32$  HRC,  $V = 182$  m/min,  $f = 0.04$  mm/rev, and  $a = 0.0833$  mm, and for Tool-3, the optimal levels were  $h = 32$  HRC,  $V = 220$  m/min,  $f = 0.04$  mm/rev, and  $a = 0.0865$  mm.
- Using the optimal inputs, it was found that the MRR for Tool-1 (with a workpiece hardness of 30 HRC), Tool-2 (with a workpiece hardness of 32 HRC), and Tool-3 (with a workpiece hardness of 32 HRC) were 639.9, 606.4, and 761.2 mm<sup>3</sup>/min, respectively. Therefore, Tool-3 has a more preferable MRR when compared to Tool-2 and Tool-1.

Overall, it can be concluded that Tool-3 was the best tool among the chosen three distinguished types of tools for the hard turning of AISI 4340 steel. In future studies, a comparative wear analysis is required to justify it more confidently.

**Author Contributions:** Conceptualization: M.R., O.İ. and M.Ö.; Investigation: M.R., O.İ., M.Ö., M.A.A., R.K. and A.P.; Experimental Test: O.İ. and M.Ö.; Methodology: M.R., O.İ., M.Ö., M.A.A., R.K. and A.P.; Software: M.R., R.K. and A.P.; Validation: M.R., R.K. and A.P.; Visualization: M.R., O.İ., M.Ö., M.A.A., R.K. and A.P.; Resources: M.R., O.İ., M.Ö., M.A.A., R.K. and A.P.; Manuscript draft preparation: M.R., O.İ., M.Ö., M.A.A., R.K. and A.P.; Paper writing, review, and editing: M.R., O.İ., M.Ö., M.A.A., R.K. and A.P. All authors have read and agreed to the published version of the manuscript.

**Funding:** The author extends their appreciation to the Deanship of Scientific Research, the King Khalid University of Saudi Arabia, for funding this work through the Large Groups Research Project under grant number (RGP. 2/163/43).

**Data Availability Statement:** The data are within this study.

**Conflicts of Interest:** The authors declare that they have no conflict of interest.

## References

1. Davim, J.P. *Machining of Hard Materials*; Springer Science & Business Media: Berlin, Germany, 2011.
2. Suresh, R.; Basavarajappa, S.; Gaitonde, V.N.; Samuel, G.; Davim, J.P. State-of-the-art research in machinability of hardened steels. *Proc. Inst. Mech. Eng. Part B J. Eng. Manuf.* **2013**, *227*, 191–209. [[CrossRef](#)]
3. Rashid, W.B.; Goel, S.; Davim, J.P.; Joshi, S.N. Parametric design optimization of hard turning of AISI 4340 steel (69 HRC). *Int. J. Adv. Manuf. Technol.* **2016**, *82*, 451–462. [[CrossRef](#)]
4. Mondal, K.; Das, S.; Mandal, B.; Sarkar, D.; Sarkar, D. An Investigation on Turning Hardened Steel Using Different Tool Inserts. *Mater. Manuf. Process.* **2016**, *31*, 1770–1781. [[CrossRef](#)]
5. Goindi, G.S.; Sarkar, P. Dry machining: A step towards sustainable machining—Challenges and future directions. *J. Clean. Prod.* **2017**, *165*, 1557–1571. [[CrossRef](#)]
6. Davim, J.P. *Machining: Fundamentals and Recent Advances*; Springer: Cham, Switzerland, 2008.
7. Sharma, N.; Gupta, K. Influence of coated and uncoated carbide tools on tool wear and surface quality during dry machining of stainless steel 304. *Mater. Res. Express* **2019**, *6*, 086585. [[CrossRef](#)]
8. Kaladhar, M. Parametric Optimization and Modeling for Flank Wear of TiSiN-TiAlN Nanolaminate Cutting Insert. *JMechE* **2021**, *17*, 69–84. [[CrossRef](#)]
9. Saikaew, C.; Paengchit, P.; Wisitsoraat, A. Machining performances of TiN+ AlCrN coated WC and Al<sub>2</sub>O<sub>3</sub>+ TiC inserts for turning of AISI 4140 steel under dry condition. *J. Manuf. Process.* **2020**, *50*, 412–420. [[CrossRef](#)]
10. Asiltürk, I.; Akkuş, H. Determining the effect of cutting parameters on surface roughness in hard turning using the Taguchi method. *Measurement* **2011**, *44*, 1697–1704. [[CrossRef](#)]
11. Ulas, H.B. Experimental Determination of Cutting Forces and Surface Roughness when Turning 50CrV4 Steel (SAE 6150) and Modelling with the Artificial Neural Network Approach. *Trans. Indian Inst. Met.* **2014**, *67*, 869–879. [[CrossRef](#)]

12. Kumar, R.; Sahoo, A.K.; Mishra, P.C.; Das, R.K. Comparative investigation towards machinability improvement in hard turning using coated and uncoated carbide inserts: Part I Experimental investigation. *Adv. Manuf.* **2018**, *6*, 52–70. [[CrossRef](#)]
13. Suresh, R.; Basavarajappa, S.; Samuel, G. Some studies on hard turning of AISI 4340 steel using multilayer coated carbide tool. *Measurement* **2012**, *45*, 1872–1884. [[CrossRef](#)]
14. Şahinoğlu, A.; Rafighi, M. Optimization of cutting parameters with respect to roughness for machining of hardened AISI 1040 steel. *Mater. Test.* **2020**, *62*, 85–95. [[CrossRef](#)]
15. Szczotkarz, N.; Maruda, R.W.; Dębowski, D.; Leksycki, K.; Wojciechowski, S.; Khanna, N.; Królczyk, G.M. Formation of Surface Topography During Turning of AISI 1045 Steel Considering the Type of Cutting Edge Coating. *Adv. Sci. Technol. Res. J.* **2021**, *15*, 253–266. [[CrossRef](#)]
16. DAS, S.R.; Panda, A.; Dhupal, D. Experimental investigation of surface roughness, flank wear, chip morphology and cost estimation during machining of hardened AISI 4340 steel with coated carbide insert. *Mech. Adv. Mater. Mod. Process.* **2017**, *3*, 305. [[CrossRef](#)]
17. Thakur, A.; Gangopadhyay, S. Evaluation of micro-features of chips of Inconel 825 during dry turning with uncoated and chemical vapour deposition multilayer coated tools. *Proc. Inst. Mech. Eng. Part B J. Eng. Manuf.* **2018**, *232*, 979–994. [[CrossRef](#)]
18. Mir, M.J.; Wani, M. Performance evaluation of PCBN, coated carbide and mixed ceramic inserts in finish-turning of AISI D2 steel. *J. Tribol.* **2017**, *14*, 10–31.
19. Abbas, A.T.; El Rayes, M.M.; Luqman, M.; Naeim, N.; Hegab, H.; Elkaseer, A. On the Assessment of Surface Quality and Productivity Aspects in Precision Hard Turning of AISI 4340 Steel Alloy: Relative Performance of Wiper vs. Conventional Inserts. *Materials* **2020**, *13*, 2036. [[CrossRef](#)]
20. Mallick, R.; Kumar, R.; Panda, A.; Sahoo, A.K. Hard Turning Performance Evaluation Using CVD and PVD Coated Carbide Tools: A Comparative Study. *Surf. Rev. Lett.* **2022**, *29*, 2250020. [[CrossRef](#)]
21. Das, A.; Kamal, M.; Das, S.R.; Patel, S.K.; Panda, A.; Rafighi, M.; Biswal, B.B. Comparative assessment between AlTiN and AlTiSiN coated carbide tools towards machinability improvement of AISI D6 steel in dry hard turning. *Proc. Inst. Mech. Eng. Part C J. Mech. Eng. Sci.* **2022**, *236*, 3174–3197. [[CrossRef](#)]
22. Boing, D.; de Oliveira, A.J.; Schroeter, R.B. Evaluation of wear mechanisms of PVD and CVD coatings deposited on cemented carbide substrates applied to hard turning. *Int. J. Adv. Manuf. Technol.* **2020**, *106*, 5441–5451. [[CrossRef](#)]
23. Varghese, V.; Ramesh, M.R.; Chakradhar, D.; Shaik, H. Characterisation and performance evaluation of TiSiN & TiAlSiN coatings by RF magnetron sputtering deposition during end milling of maraging steel. *Mater. Res. Express* **2020**, *6*, 126440. [[CrossRef](#)]
24. Sousa, V.F.; Silva, F.; Alexandre, R.; Fecheira, J. Study of the wear behaviour of TiAlSiN and TiAlN PVD coated tools on milling operations of pre-hardened tool steel. *Wear* **2021**, *476*, 203695. [[CrossRef](#)]
25. Bag, R.; Panda, A.; Sahoo, A.K.; Kumar, R. A Comprehensive Review on AISI 4340 Hardened Steel: Emphasis on Industry Implemented Machining Settings, Implications, and Statistical Analysis. *Int. J. Integr. Eng.* **2020**, *12*, 61–82. [[CrossRef](#)]
26. Savkovic, B.; Kovac, P.; Dudić, B.; Rodić, D.; Taric, M.; Gregus, M. Application of an adaptive “neuro-fuzzy” inference system in modeling cutting temperature during hard turning. *Appl. Sci.* **2019**, *9*, 3739. [[CrossRef](#)]
27. De Lima, J.G.; De Ávila, R.F.; Abrao, A. Turning of hardened AISI 4340 steel using coated carbide inserts. *Proc. Inst. Mech. Eng. Part B J. Eng. Manuf.* **2007**, *221*, 1359–1366. [[CrossRef](#)]
28. Çydaş, U. Machinability evaluation in hard turning of AISI 4340 steel with different cutting tools using statistical techniques. *Proc. Inst. Mech. Eng. Part B J. Eng. Manuf.* **2010**, *224*, 1043–1055. [[CrossRef](#)]
29. Ng, E.-G.; Aspinwall, D.K. The Effect of Workpiece Hardness and Cutting Speed on the Machinability of AISI H13 Hot Work Die Steel When Using PCBN Tooling. *J. Manuf. Sci. Eng.* **2002**, *124*, 588–594. [[CrossRef](#)]
30. Kumar, R.; Sahoo, A.K.; Mishra, P.C.; Das, R.K. Comparative study on machinability improvement in hard turning using coated and uncoated carbide inserts: Part II modeling, multi-response optimization, tool life, and economic aspects. *Adv. Manuf.* **2018**, *6*, 155–175. [[CrossRef](#)]
31. Anand, A.; Behera, A.K.; DAS, S.R. An overview on economic machining of hardened steels by hard turning and its process variables. *Manuf. Rev.* **2019**, *6*, 4. [[CrossRef](#)]
32. Bensouilah, H.; Aouici, H.; Meddour, I.; Yallese, M.A.; Mabrouki, T.; Girardin, F. Performance of coated and uncoated mixed ceramic tools in hard turning process. *Measurement* **2016**, *82*, 1–18. [[CrossRef](#)]
33. Kumar, R.; Sahoo, A.K.; Mishra, P.C.; Das, R.K. Measurement and machinability study under environmentally conscious spray impingement cooling assisted machining. *Measurement* **2019**, *135*, 913–927. [[CrossRef](#)]
34. Kumar, R.; Sahoo, A.K.; Mishra, P.C.; Das, R.K. Influence of Al<sub>2</sub>O<sub>3</sub> and TiO<sub>2</sub> nanofluid on hard turning performance. *Int. J. Adv. Manuf. Technol.* **2020**, *106*, 2265–2280. [[CrossRef](#)]
35. Shokoohi, Y.; Khosrojerdi, E.; Shiadhi, B.R. Machining and ecological effects of a new developed cutting fluid in combination with different cooling techniques on turning operation. *J. Clean. Prod.* **2015**, *94*, 330–339. [[CrossRef](#)]
36. Öztürk, B.; Kara, F. Calculation and estimation of surface roughness and energy consumption in milling of 6061 alloy. *Adv. Mater. Sci. Eng.* **2020**, *2020*, 5687951. [[CrossRef](#)]
37. Davim, J.P. *Statistical and Computational Techniques in Manufacturing*; Springer Science & Business Media: Berlin, Germany, 2012.
38. Davim, J.P.; Aveiro, P. *Design of Experiments in Production Engineering*; Springer: Cham, Switzerland, 2016.
39. Savković, B.; Kovač, P.; Stoić, A.; Dudić, B. Optimization of Machining Parameters Using the Taguchi and ANOVA Analysis in the Face Milling of Aluminum Alloys AL7075. *Teh. Vjesn. -Tech. Gaz.* **2020**, *27*, 1221–1228. [[CrossRef](#)]

40. Pahlavani, M.; Marzbanrad, J.; Rahmatabadi, D.; Hashemi, R.; Bayati, A. A comprehensive study on the effect of heat treatment on the fracture behaviors and structural properties of Mg-Li alloys using RSM. *Mater. Res. Express* **2019**, *6*, 076554. [[CrossRef](#)]
41. Moradi, M.; Aminzadeh, A.; Rahmatabadi, D.; Rasouli, S.A. Statistical and Experimental Analysis of Process Parameters of 3D Nylon Printed Parts by Fused Deposition Modeling: Response Surface Modeling and Optimization. *J. Mater. Eng. Perform.* **2021**, *30*, 5441–5454. [[CrossRef](#)]
42. Huang, Y.; Liang, S.Y. Modeling of Cutting Forces Under Hard Turning Conditions Considering Tool Wear Effect. *J. Manuf. Sci. Eng.* **2005**, *127*, 262–270. [[CrossRef](#)]
43. Fnides, B.; Yaltese, M. Cutting forces and surface roughness in hard turning of hot work steel X38CrMoV5-1 using mixed ceramic. *Mechanics* **2008**, *70*, 73–78.
44. Bartarya, G.; Choudhury, S. Effect of Cutting Parameters on Cutting Force and Surface Roughness during Finish Hard Turning AISI52100 Grade Steel. *Procedia CIRP* **2012**, *1*, 651–656. [[CrossRef](#)]
45. Aouici, H.; Yaltese, M.A.; Chaoui, K.; Mabrouki, T.; Rigal, J.-F. Analysis of surface roughness and cutting force components in hard turning with CBN tool: Prediction model and cutting conditions optimization. *Measurement* **2012**, *45*, 344–353. [[CrossRef](#)]
46. Bouziane, A.; Boulanouar, L.; Azizi, M.W.; Keblouti, O.; Belhadi, S. Analysis of cutting forces and roughness during hard turning of bearing steel. *Struct. Eng. Mech.* **2018**, *66*, 285–294.
47. Chinchankar, S.; Choudhury, S. Effect of work material hardness and cutting parameters on performance of coated carbide tool when turning hardened steel: An optimization approach. *Measurement* **2013**, *46*, 1572–1584. [[CrossRef](#)]
48. Thangarasu, S.K.; Shankar, S.; Mohanraj, T.; Devendran, K. Tool wear prediction in hard turning of EN8 steel using cutting force and surface roughness with artificial neural network. *Proc. Inst. Mech. Eng. Part C J. Mech. Eng. Sci.* **2020**, *234*, 329–342. [[CrossRef](#)]
49. Bhuiyan, M.S.H.; Choudhury, I.A. Review of Sensor Applications in Tool Condition Monitoring in Machining. *Compr. Mater. Process.* **2014**, *13*, 539–569. [[CrossRef](#)]
50. Hsu, T.-K.; Zeren, E. Effects of cutting edge geometry, workpiece hardness, feed rate and cutting speed on surface roughness and forces in finish turning of hardened AISI H13 steel. *Int. J. Adv. Manuf. Technol.* **2005**, *25*, 262–269. [[CrossRef](#)]
51. D’addona, D.; Raykar, S.J. Analysis of Surface Roughness in Hard Turning Using Wiper Insert Geometry. *Procedia CIRP* **2016**, *41*, 841–846. [[CrossRef](#)]
52. Bag, R.; Panda, A.; Sahoo, A.K.; Kumar, R. Sustainable High-Speed Hard Machining of AISI 4340 Steel Under Dry Environment. *Arab. J. Sci. Eng.* **2023**, *48*, 3073–3096. [[CrossRef](#)]
53. Şahinoğlu, A.; Rafighi, M.; Kumar, R. An investigation on cutting sound effect on power consumption and surface roughness in CBN tool-assisted hard turning. *Proc. Inst. Mech. Eng. Part E J. Process. Mech. Eng.* **2022**, *236*, 1096–1108. [[CrossRef](#)]
54. Tekner, Z.; Yeşilyurt, S. Investigation of the cutting parameters depending on process sound during turning of AISI 304 austenitic stainless steel. *Mater. Des.* **2004**, *25*, 507–513. [[CrossRef](#)]
55. Rafighi, M.; Özdemir, M.; Al Shehabi, S.; Kaya, M.T. Sustainable Hard Turning of High Chromium AISI D2 Tool Steel Using CBN and Ceramic Inserts. *Trans. Indian Inst. Met.* **2021**, *74*, 1639–1653. [[CrossRef](#)]
56. Sahinoğlu, A.; Rafighi, M. Machinability of Hardened AISI S1 Cold Work Tool Steel using Cubic Boron Nitride. *Sci. Iran.* **2021**, *28*, 2655–2670. [[CrossRef](#)]
57. Şahinoğlu, A.; Rafighi, M. Investigation of vibration, sound intensity, machine current and surface roughness values of AISI 4140 during machining on the lathe. *Arab. J. Sci. Eng.* **2020**, *45*, 765–778. [[CrossRef](#)]
58. Rafighi, M. Effects of shallow cryogenic treatment on surface characteristics and machinability factors in hard turning of AISI 4140 steel. *Proc. Inst. Mech. Eng. Part E: J. Process. Mech. Eng.* **2022**, *236*, 2118–2130. [[CrossRef](#)]
59. Bilga, P.S.; Singh, S.; Kumar, R. Optimization of energy consumption response parameters for turning operation using Taguchi method. *J. Clean. Prod.* **2016**, *137*, 1406–1417. [[CrossRef](#)]
60. Askarzadeh, A. A novel metaheuristic method for solving constrained engineering optimization problems: Crow search algorithm. *Comput. Struct.* **2016**, *169*, 1–12. [[CrossRef](#)]

**Disclaimer/Publisher’s Note:** The statements, opinions and data contained in all publications are solely those of the individual author(s) and contributor(s) and not of MDPI and/or the editor(s). MDPI and/or the editor(s) disclaim responsibility for any injury to people or property resulting from any ideas, methods, instructions or products referred to in the content.